

A CURVATURE-TENSOR-BASED PERCEPTUAL QUALITY METRIC FOR 3D TRIANGULAR MESHES

Fakhri Torkhani, Kai Wang, and Jean-Marc Chassery

Gipsa-lab, CNRS UMR 5216, Université de Grenoble

11 rue des Mathématiques, F-38042 Saint Martin d'Hères, France

{fakhri.torkhani, kai.wang, jean-marc.chassery}@gipsa-lab.grenoble-inp.fr

Abstract. Perceptual quality assessment of 3D triangular meshes is crucial for a variety of applications. In this paper, we present a new objective metric for assessing the visual difference between a reference triangular mesh and its distorted version produced by lossy operations, such as noise addition, simplification, compression and watermarking. The proposed metric is based on the measurement of the distance between curvature tensors of the two meshes under comparison. Our algorithm uses not only tensor eigenvalues (i.e., curvature amplitudes) but also tensor eigenvectors (i.e., principal curvature directions) to derive a perceptually-oriented tensor distance. The proposed metric also accounts for the visual masking effect of the human visual system, through a roughness-based weighting of the local tensor distance. A final score that reflects the visual difference between two meshes is obtained via a Minkowski pooling of the weighted local tensor distances over the mesh surface. We validate the performance of our algorithm on four subjectively-rated visual mesh quality databases, and compare the proposed method with state-of-the-art objective metrics. Experimental results show that our approach achieves high correlation between objective scores and subjective assessments.

Key words: 3D triangular mesh, perceptual quality, human visual system, objective metric, curvature tensor, visual masking.

1. Introduction

Three-dimensional (3D) triangular meshes have become the *de facto* standard for digital representation of 3D objects, and by now have found wide use in various applications, such as digital entertainment, medical imaging and computer-aided design [30]. As a rule, 3D triangular meshes undergo some lossy operations, like simplification, compression and watermarking. Although these operations are necessary to speed up and facilitate the transmission, storage and rendering of 3D meshes, or to enforce the copyright protection, they inevitably introduce distortion to the original, unprocessed mesh. However, such distortion might degrade the quality of service associated with the mesh model. Since end users of 3D triangular meshes are often human beings, it is thus important to derive some means to faithfully evaluate the degree of *visual distortion* introduced to a 3D mesh. Directly asking human subjects to evaluate the visual distortion is obviously unpractical in most real-world applications, as such subjective evaluation is time-consuming and

costly. Therefore, it is necessary to develop objective metrics (i.e., software tools) that can accurately predict the result of a subjective visual quality assessment of the for 3D triangular meshes [39].

Although during the last decade we have seen tremendous advance in objective image visual quality assessment [19, 34], the research on objective *mesh visual quality* (MVQ) assessment is still at its early stage, with very few metrics proposed [39]. A possible way to evaluate the perceptual quality of 3D meshes is to apply image quality metrics on 2D images generated through 3D model rendering under several pre-selected viewing positions. The first problem with this so-called *image-based* approach is how to select the viewing positions that the 2D image projections are generated from. In our opinion, a both optimum and automatic selection of such viewing positions is a very difficult problem in itself. Furthermore, researchers wonder whether it is appropriate to use 2D image quality metrics to evaluate the visual quality of 3D meshes. In order to answer this question, Rogowitz and Rushmeier [10] investigated the reliability of the image-based approach by conducting a series of experiments to compare the perceived quality of simplified 3D meshes (as presented in a series of continuous viewing positions) and of their corresponding 2D image projections. The experimental results seem to imply that the perceptual quality of 3D meshes is in general not equivalent to the visual quality of their 2D image projections.

Inspired and motivated by the results of Rogowitz's and Rushmeier's experiments, the research community is now paying more attention to the development of *model-based* MVQ metrics. This approach suggests that it would be more reasonable to relate MVQ directly to the 3D shape of the mesh model than to its 2D image projections. Similarly to the fact that PSNR (peak signal-to-noise ratio) and MSE (mean squared error) fail to capture the visual quality of an image [29], it is not surprising to see that classical mesh geometric distances (e.g., root mean squared error and Hausdorff distance) [6, 11] have been demonstrated to be irrelevant to human visual perception, and thus failing to predict the visual difference between an original mesh (also called *reference* mesh) and the distorted one [39]. In Fig. 1, we show an example where the Hausdorff distance (*HD*) fails to provide correct MVQ assessments: The Hausdorff distance between the original mesh in Fig. 1(a) and the distorted mesh in Fig. 1(b) is smaller than that between the original mesh and the distorted mesh in Fig. 1(c); however, conversely, the model of Fig. 1(c) has obviously better perceptual quality than the one shown in Fig. 1(b).

In order to develop an effective objective MVQ metric, it is necessary to make use of perceptually relevant features, and take into account some important properties of the *human visual system* (HVS). In this paper, we choose surface curvature amplitudes and principal curvature directions as perceptually relevant features. As discussed later, both features are important properties of the mesh surface that can be derived from eigendecomposition of the curvature tensor. Meanwhile, we integrate some HVS properties in the metric, in particular the *visual masking* effect. In the case of MVQ assessment and

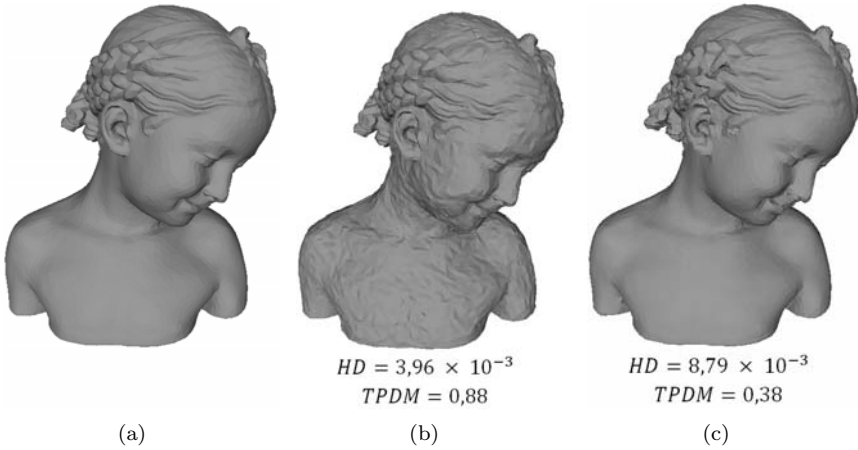


Fig. 1. (a)- Original Bimba model; (b)- Distorted Bimba with noise added in smooth regions; and (c)- Distorted Bimba with noise added in rough regions. The distortions introduced for Hausdorff distances (HD) [6,11] and $TPDM$ (Tensor-based Perceptual Distance Measure, proposed in this paper) are given below the distorted models.

as illustrated in Fig. 1, this effect mainly means that distortions in mesh surfaces are usually more visible in smooth regions than in rough regions. This paper is an extension of the earlier work presented in [36], and our contributions can be summarized as follows.

- Development of an effective model-based approach to the assessment of visual mesh quality based on a novel distance measure between mesh curvature tensors.
- Use of not only curvature amplitudes, but also of principal surface directions (which have been shown perceptually important, as discussed later) to define the curvature tensor distance.
- Integration of some HVS features in the metric: We introduce a roughness-based weighting of the local curvature tensor distance to simulate the visual masking effect, and a processing step similar to the *divisive normalization transform* to mimic an important neural mechanism, known as *adaptive gain control* [27,34].
- The source code of our MVQ metric is freely available on-line at: <http://www.gipsa-lab.fr/~fakhri.torkhani/software/TPDM.rar>.

The proposed metric, named $TPDM$ (Tensor-based Perceptual Distance Measure), has been extensively tested on four subjectively-rated visual mesh quality databases, and has been compared with state-of-the-art objective MVQ metrics. The experimental results show that our metric achieves high correlation between objective scores and subjective assessments. As a simple example to illustrate its effectiveness, $TPDM$ provides perceptually coherent assessments for the visual quality of the distorted meshes

shown in Figs. 1(b) and 1(c) (a lower *TPDM* value implies a better visual quality of the distorted model): The *TPDM* distance between the original mesh and the distorted mesh in Fig. 1(b) is 0.88, while that between the original mesh and the distorted mesh in Fig. 1(c) is 0.38. The proposed metric has the potential to be used, for instance, in the benchmarking of a variety of mesh processing algorithms (e.g., compression, watermarking, remeshing, etc.), or to guide the design of new perceptually-oriented algorithms.

The remainder of this paper is organized as follows. Related work on model-based MVQ assessment and our motivation for the design of *TPDM* are presented in Section 2. Section 3 details the pipeline of the proposed MVQ metric. The experimental results are presented in Section 4, including performance evaluation of *TPDM*, comparison with state-of-the-art MVQ metrics, and two simple examples to illustrate potential applications of the proposed metric. Finally, we draw the conclusion and suggest several future work directions in Section 5.

2. Related Work and Motivation

2.1. Model-based MVQ assessment

During the last decade, there has been increasing interest in the research on perceptual quality assessment of 3D meshes. To our knowledge, the first perceptually-oriented model-based MVQ metric was introduced by Karni and Gotsman [9] for the evaluation of their mesh compression algorithm. That metric is actually a weighted combination of root mean squared errors in vertex positions and errors in mesh Laplacian coordinates. Based on the fact that the local smoothness measure has a more important visual effect, Sorkine et al. [14] enhanced Karni and Gotsman's metric by assigning a greater weight to the errors in mesh Laplacian coordinates. Although initially proposed as by-products for evaluating mesh compression algorithms, these two metrics have triggered promising studies focusing on the perceptual quality assessment of 3D meshes.

Corsini et al. [22] developed two perceptual metrics for the visual quality assessment of watermarked meshes, named, respectively, $3DWPM_1$ and $3DWPM_2$. The visual distortion is evaluated in these two metrics as the roughness difference between the original and watermarked meshes. Two roughness measures were proposed: The first one is based on statistics (within multiscale local windows) of dihedral angles over the mesh surface, while the second roughness measure is defined as the geometric difference between a mesh model and its carefully smoothed version.

A physically-inspired MVQ metric was proposed by Bian et al. [25]. They considered 3D meshes as objects with elasticity, and assumed that the visual difference between a pair of meshes is related to the strain energy that is required to induce the deformation between them. It was shown in [25] that this metric was effective in assessing small

visual differences between meshes with constant connectivity (i.e., the same adjacency relationship between the bmesh vertices).

The research on MVQ assessment could benefit from the much more fruitful literature on image visual quality assessment. Following this line of research, Lavoué et al. [17] proposed a metric called structural mesh distortion measure (*MSDM*), which can be considered as an extension of the well-known structure similarity index for 2D images [16] to the case of 3D triangular meshes. *MSDM* relates the visual degradation to the alteration of local statistics (i.e., mean, variance and covariance) of mesh curvature amplitudes. An improved multiscale version *MSDM2* [32] has been proposed, which also integrates a vertex matching preprocessing step to allow the comparison of two meshes with different vertex connectivities.

Váša and Rus [37] proposed a dihedral angle mesh error (*DAME*) metric to compare triangular meshes sharing the same connectivity. *DAME* relies on the oriented surface dihedral angles to evaluate the perceptual distortion, and integrates the visual masking effect, as well as the visibility model which accounts for the probable viewing positions and directions of the models to be compared. This metric is computationally efficient, and has a good correlation with subjective assessment.

Recently, Wang et al. [38] introduced the fast mesh perceptual distance (*FMPD*) measure. This metric is based on a local roughness measure derived from the Gaussian curvature of the mesh surface. *FMPD* estimates the perceptual distance as the difference between the global roughness values of the two meshes under comparison. Therefore, the metric does not require a mesh correspondence or registration preprocessing step, and can be applied to compare meshes with different connectivities. *FMPD* is in essence a *reduced-reference* metric, since only the global roughness of the original mesh and some parameter values are required to carry out the visual quality assessment of a distorted mesh. In contrast, *full-reference* MVQ metrics, such as *MSDM*, *MSDM2* and *DAME*, require the availability of full information about the original mesh.

A summary of the most representative model-based MVQ metrics, along with our *TPDM* metric, is presented in Tab. 1. In that table, we also list two popular mesh geometric distances *RMS* (root mean squared error) and *HD* (Hausdorff distance). Despite their poor correlation with human visual perception [39], nowadays *RMS* and *HD* are still largely used in the evaluation of various mesh processing algorithms. The metrics are summarized according to three different algorithmic aspects: the mesh feature used for MVQ assessment, the information about the reference mesh required (i.e., whether the metric is classified as full-reference or reduced-reference one), and whether the metric requires the two meshes under comparison to have the same connectivity. Quantitative comparisons of these metrics are presented in Section 4.

Tab. 1. Summary of model-based mesh perceptual quality metrics.

| Metric | Feature | Information about reference mesh | Connectivity constraint |
|--------------------|--------------------------------|----------------------------------|-------------------------|
| <i>RMS</i> [6, 11] | Surface-to-surface distance | Full-reference | No |
| <i>HD</i> [6, 11] | Surface-to-surface distance | Full-reference | No |
| <i>3DWPM</i> [22] | Global roughness | Reduced-reference | Yes |
| <i>MSDM</i> [17] | Curvature amplitude | Full-reference | Yes |
| <i>MSDM2</i> [32] | Multiscale curvature amplitude | Full-reference | No |
| <i>DAME</i> [37] | Dihedral angle | Full-reference | Yes |
| <i>FMPD</i> [38] | Global roughness | Reduced-reference | No |
| <i>TPDM</i> | Curvature tensor distance | Full-reference | No |

2.2. Motivation for tensor-based MVQ assessment

MSDM2 has a good correlation with subjective scores [32], though by considering only the modification in mesh curvature amplitudes. We argue that a modification in the *principal surface directions* as defined by the *orthogonal* directions of minimum and maximum curvatures is also important for MVQ assessment. As shown in Fig. 2, maximum and minimum curvature directions represent salient structural features of the surface and thus should be visually important. Indeed, when drawing a 3D object, one strategy of caricaturists is to draw strokes on these lines of curvatures [23]. For example, we may expect that the drawings of either trained artists or untrained amateurs, when asked to complete a line drawing of the Bimba model shown in Fig. 2(a), would be similar to the images shown in Figs. 2(b) and 2(c). The perceptual importance of principal surface directions have been noticed by computer graphics and geometry processing experts: They have been successfully used for describing [3] and illustrating [8] complex 3D objects, as well as for guiding a high-performance anisotropic remeshing algorithm [12].

Motivated by the above observation, in this paper we introduce a new MVQ metric *TPDM* which makes use of more information that can be extracted from mesh curvature tensors, i.e., both the curvature amplitudes and the principal surface directions. In Section 4, we will show that experimentally our tensor-based metric achieves a high correlation with the subjective scores of mesh visual quality. In particular, the use of information on principal surface directions in *TPDM* appears to help improve the assessment performance when compared to the state-of-the-art metric *MSDM2* that uses only curvature amplitudes. Before presenting the technical details of the proposed metric in Section 3, in the next subsection we will briefly introduce a technique for the estimation of mesh curvature tensors, and explain how to obtain curvature amplitudes and principal curvature directions from the tensor.

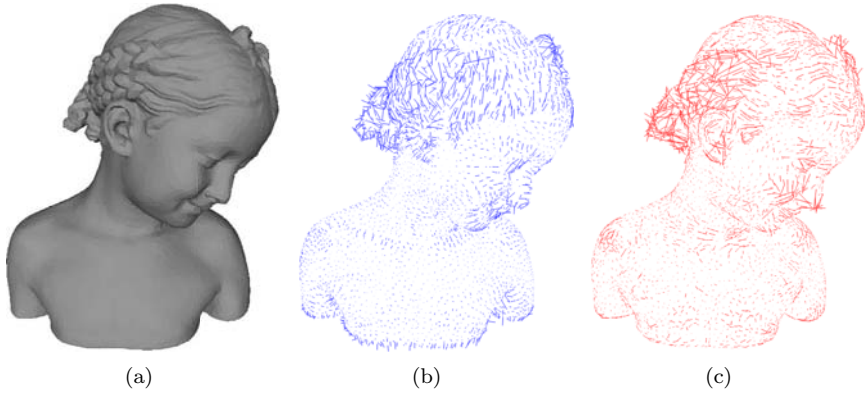


Fig. 2. (a)- Bimba’s model; (b)- Maximum curvature directions of Bimba scaled by maximum curvature values; and (c)- Minimum curvature directions of Bimba scaled by minimum curvature values.

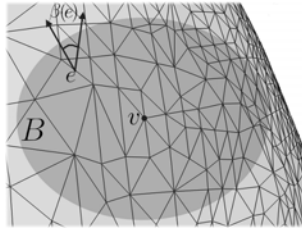


Fig. 3. Geometric elements used to compute the curvature tensor.

2.3. Curvature tensor estimation

Estimation of the mesh curvature tensor is a well-researched problem. So far, the most popular estimation technique has been the one from Cohen-Steiner and Morvan [13]. Based on the solid foundation of normal cycle theory, they derived an elegant per-vertex curvature tensor estimation. Tensors computed on edges are averaged on a geodesic disk window B of user-defined size to obtain the curvature tensor \mathcal{T} on each vertex v :

$$\mathcal{T}(v) = \frac{1}{|B|} \sum_{\text{edges } e} \beta(e) |e \cap B| \bar{e} \bar{e}^t, \tag{1}$$

where $|B|$ is the area of the geodesic disk, $\beta(e)$ is the signed angle between the normals of the two triangles incident to edge e , $|e \cap B|$ is the length of the part of e inside B , \bar{e} and \bar{e}^t are the unit vector in the direction of e and its transpose (cf. Fig. 3), respectively. The minimum and maximum curvature amplitudes (denoted by κ_{min} and

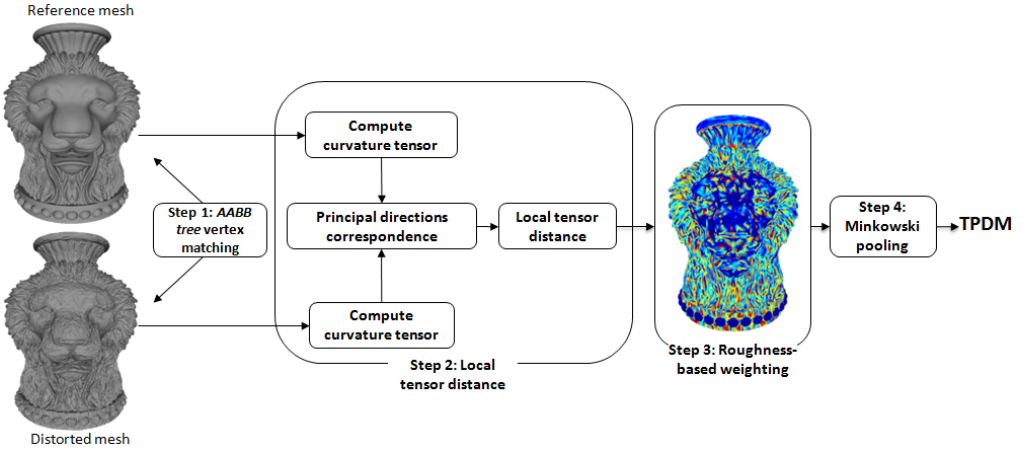


Fig. 4. Block diagram of the pipeline of *TPDM* (Tensor-based Perceptual Distance Measure). In the roughness map within the block of “Step 3: Roughness-based weighting”; warmer colors represent larger values (i.e., where the local surface is rougher).

κ_{max}), respectively) are the absolute values of the two non-zero eigenvalues of the tensor \mathcal{T} , and the principal surface directions are the associated two eigenvectors (denoted by 3D vectors γ_{min} and γ_{max} , respectively). In Section 3, we will derive a perceptually-oriented distance between curvature tensors by incorporating the information from both their eigenvalues and their eigenvectors, and will use this distance to conduct the MVQ assessment.

3. MVQ Assessment Based on Curvature Tensor Distance

An overview of the processing pipeline for the proposed MVQ metric *TPDM* is illustrated in Fig. 4. First of all, in order to compare two meshes with potentially different connectivities, we perform a preprocessing step of vertex matching between the two meshes under comparison, based on the AABB tree data structure implemented in the CGAL library [35]. The objective of this step is to find, for each vertex of the reference mesh, a corresponding point on the surface of the distorted mesh. The second step is to compute a curvature tensor at each vertex of the two meshes, and then to derive the distance between the tensors of each vertex in the reference mesh and its counterpart in the distorted mesh. Both the curvature amplitudes and the principal curvature directions are involved in the tensor distance calculation. Before this local tensor distance computation, a correspondence relationship has to be established between the principal curvature directions and the curvature amplitudes of the two tensors to be compared,

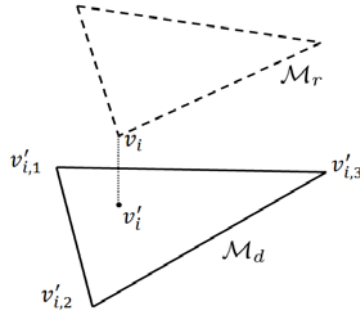


Fig. 5. Projection of a vertex v_i of the reference mesh \mathcal{M}_r onto the surface of the distorted mesh \mathcal{M}_d . Here the projection is v'_i , a point on the triangular facet that is constituted of $v'_{i,1}$, $v'_{i,2}$ and $v'_{i,3}$. For the sake of simplicity, we only show one single facet in \mathcal{M}_r and in \mathcal{M}_d .

so as to determine for each vertex how to exactly calculate the tensor distance. In the third step, this local tensor distance is weighted by two roughness-based factors in order to account for the visual masking effect of HVS, which is vital for conducting a correct MVQ assessment. In the fourth and last step, we use a surface-weighted Minkowski pooling of the local $TPDM$ distances to obtain a global $TPDM$ value. In what follows, we will present the technical details of each of the four steps.

3.1. Vertex matching preprocessing

In order to establish the correspondence between the vertices of the two meshes, analogously as in the preprocessing step in *MSDM2* [32], we use the AABB tree data structure implemented in the CGAL library [35] to perform a fast and simple vertex projection from the reference mesh \mathcal{M}_r to the surface of the distorted mesh \mathcal{M}_d . As a result of this matching step, each vertex v_i in \mathcal{M}_r is assigned a corresponding point v'_i on the surface of \mathcal{M}_d . Note that v'_i is in general not a vertex of \mathcal{M}_d , but a point on a certain triangular facet T'_i of \mathcal{M}_d composed of three vertices $v'_{i,1}$, $v'_{i,2}$ and $v'_{i,3}$ (cf. Fig. 5). In this general case, the local $TPDM$ distance associated to v_i , denoted by $LTPDM_{v_i}$, is computed as the barycentric interpolation [2] of the three local perceptual distances, between v_i and $v'_{i,1}$, v_i and $v'_{i,2}$, and finally v_i and $v'_{i,3}$, respectively:

$$LTPDM_{v_i} = \sum_{k=1}^3 b_k(v'_i) LPD_{v_i, v'_{i,k}}, \tag{2}$$

where $LPD_{v_i, v'_{i,k}}$ is the local perceptual distance between v_i and the k -th vertex of the triangular facet T'_i that contains the projection v'_i , and $b_k(v'_i)$ is the k -th barycentric coordinate [2] of v'_i within T'_i . The next two subsections focus on how to derive the local perceptual distance $LPD_{v_i, v'_{i,k}}$.

3.2. Local tensor distance

The derivation of the local perceptual distances $LPD_{v_i, v'_{i,k}}$ is based on the local tensor distances between v_i and $v'_{i,k}$, denoted by $LTD_{v_i, v'_{i,k}}$ for $k = 1, 2, 3$. For this purpose, we first estimate the curvature tensors at each vertex of \mathcal{M}_r and \mathcal{M}_d . The tensors on the two vertices v_i and $v'_{i,k}$ are hereafter denoted by \mathcal{T}_{v_i} and $\mathcal{T}_{v'_{i,k}}$, respectively. They are computed using Equation (1), with a local window established as the intersection of the mesh surface and the Euclidean sphere [13] that is centered on the vertex and has, experimentally, a radius equal to 0.5% of the bounding box diagonal of \mathcal{M}_r .

As mentioned earlier, we want to use the differences between both the curvature amplitudes (i.e., tensor eigenvalues) and the principal curvature directions (i.e., tensor eigenvectors) to derive the local tensor distance. We should first of all decide between which curvature amplitudes/directions we will compute the differences. The straightforward choice is to derive the difference between the minimum curvature of \mathcal{T}_{v_i} and the minimum curvature of $\mathcal{T}_{v'_{i,k}}$ (the same for the differences in the maximum curvature amplitudes, in the minimum curvature directions and in the maximum curvature directions). Then we can combine the obtained four differences to derive the local tensor distance. However, we find that this simple “min→min, max→max” correspondence between the tensor elements results in poor MVQ assessments, especially in the situations where the principal directions are severely disturbed after medium and strong distortions, and where the mesh contains a large portion of locally isotropic regions (in these regions, the values of minimum and maximum curvature amplitudes are close to each other, so that the minimum and maximum curvatures may change roles even after small-amplitude distortions).

Motivated by this observation, we adopt another rule for establishing the correspondence relationship between the curvature amplitudes/directions of \mathcal{T}_{v_i} and $\mathcal{T}_{v'_{i,k}}$, which is based on the *minimum angular distance criterion* between the principle curvature directions. More precisely, for γ_{min} (i.e., the minimum curvature direction) of \mathcal{T}_{v_i} , we find the principal direction of $\mathcal{T}_{v'_{i,k}}$ that has the smallest angular distance to it (this direction is denoted by γ'_1), and then relate γ_{min} to γ'_1 . Accordingly, κ_{min} (i.e., the minimum curvature amplitude) of \mathcal{T}_{v_i} is related to the curvature amplitude associated to γ'_1 (denoted by κ'_1). That is, if γ'_1 is the minimum (or maximum) curvature direction of $\mathcal{T}_{v'_{i,k}}$, then κ'_1 is the minimum (or maximum) curvature amplitude of $\mathcal{T}_{v'_{i,k}}$. Under the proposed correspondence rule, γ'_1 can be either the minimum or the maximum curvature direction of $\mathcal{T}_{v'_{i,k}}$, as long as this minimum or maximum curvature direction has the smallest angular distance to γ_{min} . Similarly, the following correspondence relationships are established: $\kappa_{max} \rightarrow \kappa'_2$ and $\gamma_{max} \rightarrow \gamma'_2$. It is easy to see that γ'_1 and γ'_2 (and κ'_1 and κ'_2 , respectively) are distinct principal curvature directions (distinct principal curvature amplitudes, respectively) of $\mathcal{T}_{v'_{i,k}}$. In practice, the above correspondence, which is based

on the minimum angular distance criterion, yields better MVQ assessment results than the straightforward “min→min, max→max” correspondence discussed above.

The local tensor distance is computed for each pair of v_i and $v'_{i,k}$ as

$$LTD_{v_i, v'_{i,k}} = \frac{\theta_{min}}{(\pi/2)} \delta_{\kappa_{min}} + \frac{\theta_{max}}{(\pi/2)} \delta_{\kappa_{max}}, \quad (3)$$

where $\theta_{min} \in [0, \pi/2]$ is the angle between the curvature lines of γ_{min} and γ'_1 (similarly, $\theta_{max} \in [0, \pi/2]$ is the angle between the lines of γ_{max} and γ'_2), and $\delta_{\kappa_{min}}$ is a Michelson-like contrast [1] of the curvature amplitudes κ_{min} and κ'_1 , i.e., $\delta_{\kappa_{min}} = \left| \frac{\kappa_{min} - \kappa'_1}{\kappa_{min} + \kappa'_1 + \varepsilon} \right|$ with ε a stabilization constant fixed as 5% of the average mean curvature of \mathcal{M}_r (similarly, $\delta_{\kappa_{max}} = \left| \frac{\kappa_{max} - \kappa'_2}{\kappa_{max} + \kappa'_2 + \varepsilon} \right|$). Both the differences in the curvature amplitudes and in the principal surface directions are involved in the derivation of the local tensor distance. Besides its perceptual relevance [4, 5], another reason to use the Michelson-like contrast to evaluate the difference between curvature amplitudes is that in this way both the difference the principal directions (after the normalization by a factor of $\pi/2$) and in the curvature amplitudes are in the same range of $[0, 1]$, so that these two kinds of differences can be easily combined together.

3.3. Roughness-based weighting of local tensor distance

For the development of an effective MVQ metric, we should take into account some HVS features, in particular the visual masking effect [20]. In the context of MVQ assessment, this effect mainly means that the same distortion is less visible in rough regions of the mesh surface than in the smooth regions. In order to account for the visual masking effect, our solution is to modulate the values of $LTD_{v_i, v'_{i,k}}$ by two roughness-based weights (the rougher the local surface is, the smaller the weights are). The local perceptual distance between v_i and $v'_{i,k}$, which incorporates the visual masking effect, is computed as:

$$LPD_{v_i, v'_{i,k}} = RW_i^{(\gamma)} \cdot RW_i^{(\kappa)} \cdot LTD_{v_i, v'_{i,k}}, \quad (4)$$

with $RW_i^{(\gamma)}, RW_i^{(\kappa)} \in [0.1, 1.0]$. They are, respectively, the roughness-based weights derived from the principal surface directions and the curvature amplitudes in the 1-ring neighborhood of v_i . For $RW_i^{(\gamma)}$, we first project all the principal curvature directions at the 1-ring neighbors of v_i on the tangent plane of v_i , and then take the sum of the two angular standard deviations of the projected minimum and maximum curvature directions as the local roughness value. This value is then linearly mapped to $[0.1, 1.0]$ to obtain $RW_i^{(\gamma)}$: The higher the sum of the two angular standard deviations is, the lower the mapped value is. Similarly, to get $RW_i^{(\kappa)}$, we compute the ratio of the Laplacian for the mean curvatures in the 1-ring neighborhood of v_i and the mean curvature at v_i as the

local roughness measure. The Laplacian of the mean curvatures in the 1-ring neighborhood of v_i describes the local variation of the mesh curvature amplitudes. In our metric, we use the cotangent-based mesh Laplacian due to its solid theoretical foundation and its excellent performance in practical applications [18, 24]. This curvature-amplitude-based roughness value is then linearly mapped to $[0.1, 1.0]$ to obtain $RW_i^{(\kappa)}$: The higher the roughness is, the lower the mapped value is. It is worth mentioning that the derivation of the roughness weight $RW_i^{(\kappa)}$ includes a divisive normalization (i.e., the normalization of the Laplacian for mean curvatures by the mean curvature on v_i itself), which is similar to that in the neural mechanism of HVS that partially explains the visual masking effect [27, 34]. Also note that vertices in isotropic regions, i.e., where κ_{min} and κ_{max} are close to each other, are treated differently. An anisotropy coefficient ρ_{v_i} is first computed as:

$$\rho_{v_i} = \frac{\kappa_{max}^{(v_i)} - \kappa_{min}^{(v_i)}}{\kappa_{max}^{(v_i)} + \kappa_{min}^{(v_i)} + \epsilon}, \quad (5)$$

where $\kappa_{min}^{(v_i)}$ and $\kappa_{max}^{(v_i)}$ are, respectively, the minimum and maximum curvatures at vertex v_i , and ϵ is a stabilization constant set as 5% of the average mean curvature of \mathcal{M}_r . We consider that the vertices at which ρ_{v_i} is smaller than 0.5 belong to relatively isotropic regions. For these vertices, we set $RW_i^{(\gamma)}$ equal to 1, and accordingly the final roughness-based weight is determined by the value of $RW_i^{(\kappa)}$. The reason is that in isotropic regions, the principal curvature directions are not well-defined and their estimation is not reliable. It is therefore safer to use only the curvature-amplitude-based roughness weight $RW_i^{(\kappa)}$ for the local tensor distance modulation. A roughness map that combines both weights $RW_i^{(\gamma)}$ and $RW_i^{(\kappa)}$ is shown in the ‘‘Step 3’’ block of Fig. 4, where warmer colors represent higher roughness values (i.e., lower roughness-based weights).

Finally, as described by Equation (2), the local tensor-based perceptual distance measure at vertex v_i , $LTPDM_{v_i}$, is computed as the barycentric interpolation of the three local perceptual distances $LPD_{v_i, v'_{i,1}}$, $LPD_{v_i, v'_{i,2}}$ and $LPD_{v_i, v'_{i,3}}$.

3.4. Global perceptual distance

The global tensor-based perceptual distance measure $TPDM$ from the reference mesh \mathcal{M}_r to the distorted mesh \mathcal{M}_d is computed as the *weighted Minkowski sum* of the local distances $LTPDM_{v_i}$, $i = 1, 2, \dots, N$:

$$TPDM = \left(\sum_{i=1}^N w_i |LTPDM_{v_i}|^p \right)^{\frac{1}{p}}, \quad (6)$$

where $w_i = s_i / \sum_{i=1}^N s_i$ with s_i one third of the total area of all the incident facets of v_i , and $p = 2.5$. The surface-based weighting can, to some extent, enhance the stability of

the metric to the variation of vertex sampling density over the mesh surface. Compared to the standard mean-squared error where $p = 2.0$, the choice of $p = 2.5$ can increase the importance of the local high amplitude distances of in the calculation of the global perceptual distance [15]. This is perceptually relevant, since the part of mesh with high-amplitude distortion experimentally attracts more attention from human observers, and thus has more impact on the result of subjective assessment.

4. Experimental Results

4.1. Performance evaluation and comparisons

In order to verify its efficacy, the proposed metric *TPDM* has been extensively tested and compared with the existing metrics on four subjectively-rated visual mesh quality databases:

- The LIRIS/EPFL general-purpose database¹ [17]: Contains 4 reference meshes and the total of 84 distorted models. The distortion types include noise addition and smoothing, applied either locally or globally to the reference mesh. Subjective evaluations were made by 12 observers.
- The LIRIS masking database² [26]: Contains 4 reference meshes and the total of 24 distorted models. The local noise addition distortion included in this database was designed specifically for testing the capability of MVQ metrics to capture the visual masking effect. 11 observers participated in the subjective tests.
- The IEETA simplification database³ [28]: Contains 5 reference meshes and the total of 30 simplified models. 65 observers participated in the subjective study.
- The UWB compression database⁴ [37]: Contains 5 reference meshes and the total of 64 distorted models. Subjective evaluations were made by 69 observers.

TPDM has been compared with seven state-of-the-art metrics, i.e., the Hausdorff distance (*HD*) [6, 11], the root mean squared error (*RMS*) [6, 11], *3DWPM*₁ and *3DWPM*₂ [22], *MSDM*₂ [32], *DAME* [37] and *FMPD* [38]. The coherence between the objective values produced by the MVQ metrics and the mean opinion scores (*MOS*) provided by subjective databases is measured using two different correlation kinds: The Pearson linear correlation coefficient (*PLCC* or r_p), which measures the prediction accuracy of the objective metrics, and the Spearman rank-order correlation coefficient (*SROCC* or r_s), which measures the prediction monotonicity [19, 34]. Before computing the correlation values, especially the *PLCC*, it is recommended to conduct a psychometric fitting between the objective scores and the *MOS* values, in order to partially

¹<http://liris.cnrs.fr/guillaume.lavoue/data/datasets.html>

²<http://liris.cnrs.fr/guillaume.lavoue/data/datasets.html>

³<http://www.ieeta.pt/~sss/index.php/perceivedquality/repository>

⁴<http://compression.kiv.zcu.cz/>

remove the non-linearity between them. Another effect of psychometric fitting is that afterwards we obtain objective MVQ values belonging to the $[0, 1]$ interval, which are easier for the users to understand. In our tests, we apply a cumulative Gaussian psychometric function [7] for the fitting:

$$g(a, b, R) = \frac{1}{\sqrt{2\pi}} \int_{a+bR}^{\infty} e^{-(t^2/2)} dt, \quad (7)$$

where R is the raw *TPDM* value. The two parameters $a = -1.14$ and $b = 11.47$ are obtained through a non-linear least squares fitting (under Matlab, with the curve fitting toolbox) using the raw *TPDM* values and the corresponding *MOS* for the group of Dinosaur models in the general-purpose database. As shown in Fig. 6, the same psychometric function is used for models in other subjective databases. From the plots we can see that the fitted psychometric function has a good generalization capability for other databases, as the psychometric curve is close to the *TPDM-MOS* pairs.

The tables 2 to 5 present, respectively, the evaluation and comparison results for the general-purpose, masking, simplification and compression databases. Analogously to the comparisons in [39], the overall correlations (last two columns in the tables) are computed for the whole database (i.e., we compute the statistical linear or non-linear dependence between all objective scores and *MOS* values of all models in each database), except the compression database, where per-model averages are used. This is because the data acquisition procedure of the compression database does not take into account inter-model coherence [37, 39]. The results for the existing metrics shown in Tabs. 2 to 5 are either extracted from published papers [31, 37–39] and the related erratum [40], or collected from our own tests.

The geometric distance metrics *HD* and *RMS* in general fail to evaluate the perceptual mesh quality: The overall Pearson and Spearman correlations are quite low for all the four databases. *HD* even results in a negative correlation on some difficult models, i.e., *Jessy* and *James* from the compression database (cf. Tab. 5). In the following we will focus on the comparison of our approach with state-of-the-art perceptually-driven MVQ metrics for each database.

For the general-purpose database (cf. Tab. 2), *TPDM* has high *PLCC* and *SROCC* values for almost every individual model, as well as for the whole repository. *TPDM* has the highest overall *PLCC* and *SROCC* values among all the MVQ metrics tested (the last two columns). In particular, there is a noticeable improvement in terms of overall correlations compared to the second best metric *FMPD*. For example, the overall *SROCC* has improved from 81.9% for *FMPD* to 89.6% for *TPDM*. Since the general-purpose database has the highest number of distorted models among the four available databases, as well as a variety of distortion types, the high correlation values of *TPDM* for this database appear to be promising evidence for the good performance of *TPDM* in assessing visual mesh quality.

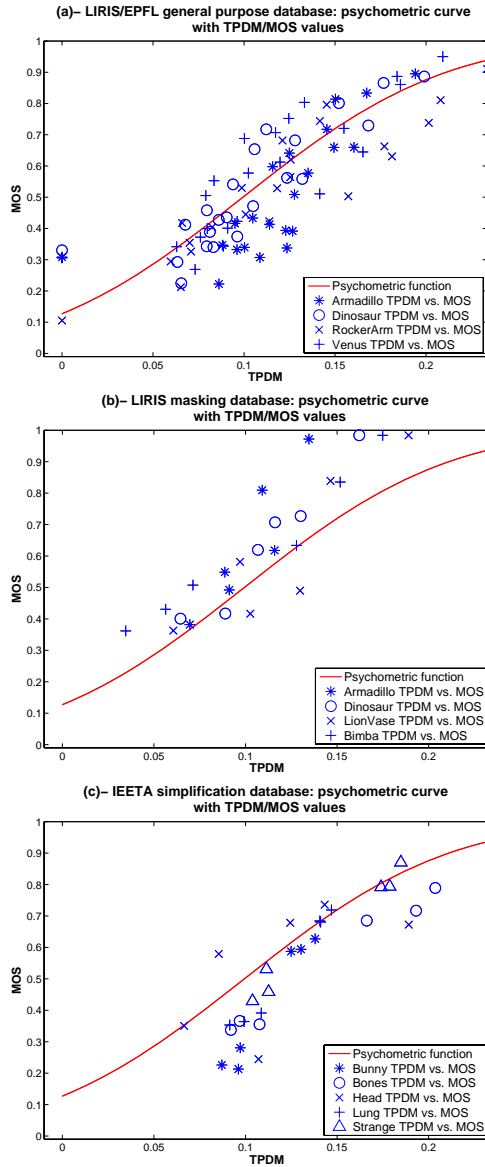


Fig. 6. Psychometric function curve plotted with *TPDM-MOS* pairs of all the reference and distorted models in: (a)- the LIRIS/EPFL general-purpose database; (b)- the LIRIS masking database; and (c)- the IEETA simplification database.

Tab. 2. $PLCC$ (r_p) and $SROCC$ (r_s) (%) of different objective metrics on the general-purpose database.

| Metric | Armadillo | | Dinosaur | | RockerArm | | Venus | | All models | |
|--------------------------------|-------------|-------------|-------------|-------------|-------------|-------------|-------------|-------------|-------------|-------------|
| | r_p | r_s |
| <i>HD</i> [6, 11] | 54.9 | 69.5 | 47.5 | 30.9 | 23.4 | 18.1 | 8.9 | 1.6 | 11.4 | 13.8 |
| <i>RMS</i> [6, 11] | 56.7 | 62.7 | 0.0 | 0.3 | 17.3 | 7.3 | 87.9 | 90.1 | 28.1 | 26.8 |
| <i>3DWPM</i> ₁ [22] | 59.7 | 65.8 | 59.7 | 62.7 | 72.9 | 87.5 | 68.3 | 71.6 | 61.9 | 69.3 |
| <i>3DWPM</i> ₂ [22] | 65.6 | 74.1 | 44.6 | 52.4 | 54.7 | 37.8 | 40.5 | 34.8 | 49.6 | 49.0 |
| <i>MSDM</i> ₂ [32] | 85.3 | 81.6 | 85.7 | 85.9 | 87.2 | 89.6 | 87.5 | 89.3 | 81.4 | 80.4 |
| <i>DAME</i> [37] | 76.3 | 60.3 | 88.9 | 92.8 | 80.1 | 85.0 | 83.9 | 91.0 | 75.2 | 76.6 |
| <i>FMPD</i> [38] | 83.2 | 75.4 | 88.9 | 89.6 | 84.7 | 88.8 | 83.9 | 87.5 | 83.5 | 81.9 |
| <i>TPDM</i> | 78.8 | 84.5 | 89.0 | 92.2 | 91.4 | 92.2 | 91.0 | 90.6 | 86.2 | 89.6 |

Tab. 3. $PLCC$ (r_p) and $SROCC$ (r_s) (%) of different objective metrics on the masking database.

| Metric | Armadillo | | Bimba | | Dinosaur | | LionVase | | All models | |
|--------------------------------|-------------|-------------|-------------|------------|-------------|------------|-------------|------------|-------------|-------------|
| | r_p | r_s | r_p | r_s | r_p | r_s | r_p | r_s | r_p | r_s |
| <i>HD</i> [6, 11] | 61.4 | 48.6 | 27.4 | 25.7 | 55.8 | 48.6 | 50.1 | 71.4 | 20.2 | 26.6 |
| <i>RMS</i> [6, 11] | 66.8 | 65.7 | 46.7 | 71.4 | 70.9 | 71.4 | 48.8 | 71.4 | 41.2 | 48.8 |
| <i>3DWPM</i> ₁ [22] | 64.6 | 58.0 | 29.0 | 20.0 | 67.3 | 66.7 | 31.1 | 20.0 | 31.9 | 29.4 |
| <i>3DWPM</i> ₂ [22] | 61.6 | 48.6 | 37.9 | 37.1 | 70.8 | 71.4 | 46.9 | 38.3 | 42.7 | 37.4 |
| <i>MSDM</i> ₂ [32] | 81.1 | 88.6 | 96.8 | 100 | 95.6 | 100 | 93.5 | 94.3 | 87.3 | 89.6 |
| <i>DAME</i> [37] | 96.0 | 94.3 | 88.0 | 97.7 | 89.4 | 82.9 | 99.5 | 100 | 58.6 | 68.1 |
| <i>FMPD</i> [38] | 94.2 | 88.6 | 98.9 | 100 | 96.9 | 94.3 | 93.5 | 94.3 | 80.8 | 80.2 |
| <i>TPDM</i> | 91.4 | 88.6 | 97.2 | 100 | 97.1 | 100 | 88.4 | 82.9 | 88.6 | 90.0 |

From the results for the masking database (cf. Tab. 3), we can see that in general *TPDM* captures the visual masking effect well, as reflected by the high individual and overall $PLCC$ and $SROCC$ values for that database. The same applies to the results for the general-purpose database: *TPDM* has the highest overall $PLCC$ and $SROCC$ values among all the metrics tested. Another observation is that although the reduced-reference metric *FMPD* performs quite well for each individual model, its overall $PLCC$ and $SROCC$ values are not that high when compared to the full-reference metrics *MSDM*₂ and *TPDM*. Hence, it seems that in order to capture the visual masking effect well in the case of MVQ assessment, it would be advantageous to conduct a precise vertex-to-vertex local analysis, with the availability of the full information about the reference mesh.

Compared to other connectivity-independent metrics (cf. Tab. 1), *TPDM* has comparable performance with *MSDM*₂ and *FMPD* for the simplification database (cf. Tab. 4). The results of *3DWPM*₁, *3DWPM*₂ and *DAME* are missing because those metrics have the mesh connectivity constraint, and therefore cannot be applied to compare two meshes with different connectivities. For the Head model, the correlation of

Tab. 4. $PLCC$ (r_p) and $SROCC$ (r_s) (%) of different objective metrics on the simplification database.

| Metric | Bones | | Bunny | | Head | | Lung | | Strange | | All models | |
|--------------------|-------------|-------------|-------------|-------------|-------------|-------------|-------------|------------|-------------|-------------|-------------|-------------|
| | r_p | r_s | r_p | r_s | r_p | r_s | r_p | r_s | r_p | r_s | r_p | r_s |
| <i>HD</i> [6, 11] | 92.0 | 94.3 | 37.8 | 39.5 | 72.8 | 88.6 | 80.6 | 88.6 | 52.3 | 37.1 | 50.5 | 49.4 |
| <i>RMS</i> [6, 11] | 86.4 | 94.3 | 94.5 | 77.1 | 49.6 | 42.9 | 89.0 | 100 | 90.4 | 88.6 | 59.6 | 70.2 |
| <i>MSDM2</i> [32] | 98.3 | 94.3 | 98.1 | 77.1 | 88.9 | 88.6 | 92.3 | 60.0 | 99.0 | 94.3 | 89.2 | 86.7 |
| <i>FMPD</i> [38] | 96.0 | 88.6 | 98.0 | 94.3 | 70.4 | 65.7 | 95.5 | 88.6 | 96.0 | 65.7 | 89.3 | 87.2 |
| <i>TPDM</i> | 99.0 | 94.3 | 98.0 | 94.3 | 63.1 | 65.7 | 98.6 | 94.3 | 98.7 | 94.3 | 86.9 | 88.2 |

Tab. 5. $PLCC$ (r_p) and $SROCC$ (r_s) (%) of different objective metrics on the compression database.

| Metric | Bunny | | James | | Jessy | | Nissan | | Helix | | All models | |
|-------------------------------|-------------|-------------|-------------|-------------|-------------|-------------|-------------|-------------|-------------|-------------|-------------|-------------|
| | r_p | r_s |
| <i>HD</i> [6, 11] | 34.1 | 52.2 | -16.8 | 6.8 | -23.6 | 12.5 | 14.4 | 23.6 | 45.1 | 46.4 | 10.6 | 28.3 |
| <i>RMS</i> [6, 11] | 34.2 | 20.9 | 14.0 | 10.8 | 0.0 | 14.8 | 17.8 | 29.7 | 46.9 | 44.6 | 22.0 | 24.1 |
| <i>3DWPM₁</i> [22] | 94.7 | 93.4 | 77.3 | 72.3 | 87.2 | 89.5 | 63.6 | 59.3 | 98.0 | 95.2 | 84.1 | 81.9 |
| <i>3DWPM₂</i> [22] | 96.0 | 91.2 | 76.9 | 65.3 | 86.9 | 85.9 | 56.3 | 67.6 | 95.5 | 94.3 | 82.3 | 80.9 |
| <i>MSDM2</i> [32] | 97.4 | 90.1 | 82.6 | 69.2 | 84.3 | 63.1 | 84.4 | 73.1 | 98.1 | 94.7 | 89.3 | 78.0 |
| <i>DAME</i> [37] | 96.8 | 93.4 | 95.7 | 93.4 | 84.4 | 70.5 | 93.9 | 75.3 | 96.6 | 95.2 | 93.5 | 85.6 |
| <i>FMPD</i> [38] | 94.2 | 89.6 | 95.3 | 91.2 | 63.3 | 60.0 | 92.4 | 77.5 | 98.4 | 90.8 | 88.8 | 81.8 |
| <i>TPDM</i> | 95.1 | 96.5 | 90.8 | 73.6 | 85.8 | 75.8 | 82.7 | 73.4 | 98.7 | 95.0 | 91.5 | 82.9 |

TPDM is rather low. This is because *TPDM* has difficulties in distinguishing the quality of simplified Head meshes generated by different simplification algorithms but with the same vertex reduction ratio. *FMPD* is more or less affected by the same problem. The simplification database is a relatively simple dataset. *MSDM2*, *FMPD* and *TPDM* all have very high overall correlation on this database, and even *HD* and *RMS* have very good performance on some individual models. This observation implies the necessity of constructing a comprehensive subjectively-rated MVQ database which incorporates more models and more types of lossy operations affecting mesh connectivity, e.g., other simplification algorithms, remeshing or even subdivision.

For the compression database (cf. Tab. 5), *DAME* has the highest overall $PLCC$ and $SROCC$: 93.5% and 85.6% for *DAME* against respectively 91.5% and 82.9% for *TPDM*, the second best metric for this database. Initially, we encountered difficulties in testing *TPDM* on the James, Jessy and Nissan models, which consist of many spatially non-connected components (70, 138 and 212, respectively). Some of the components have null Euclidean distance to each other, so that the vertex matching preprocessing fails since a vertex may be incorrectly projected onto a different nearby component, even without any introduced distortion. A simple solution has been adopted to resolve this problem. We first identify such incorrectly projected vertices on the reference mesh by

conducting the *TPDM* comparison between the reference mesh and itself. The incorrectly projected vertices are those with non-zero *LTPDM* values. When performing a comparison with a distorted mesh, the *LTPDM* distances for these vertices are deduced from the distance values of its 1-ring neighbors, via simple median filtering. This also demonstrates that in order to conduct an effective MVQ assessment (especially for the development of full-reference MVQ metrics), it is important to develop a robust, or ideally perceptually-driven, mesh correspondence algorithm. The development of such an algorithm remains an open research problem.

All in all, *TPDM* shows quite good performance on all the available subjectively-rated mesh visual quality databases, as reflected by its high correlation with subjective scores on most individual models, as well as on the whole repositories. In particular, *TPDM* has the highest overall *SROCC* (the last column in the tables) on the general-purpose, masking and simplification databases, and it is the second best performing metric on the compression database. Furthermore, *TPDM* has always higher *SROCC* than *MSDM2* on all the four databases, and also under three cases out of four higher *PLCC* values (the exception is the simplification database). It appears that the injection of the information on the principal surface directions helps improve the MVQ assessment performance.

TPDM also allows us to obtain a perceptually coherent distance map between two meshes. Figure 7 illustrates the distance maps produced by *TPDM* and *RMS* between the original Bimba model and a distorted Bimba after uniform random noise addition. The map of *TPDM* is quite consistent with human perception (i.e., the perceived distortion is higher in smooth regions than in rough regions), while the map of *RMS* is purely geometric and fails to capture the visual masking effect.

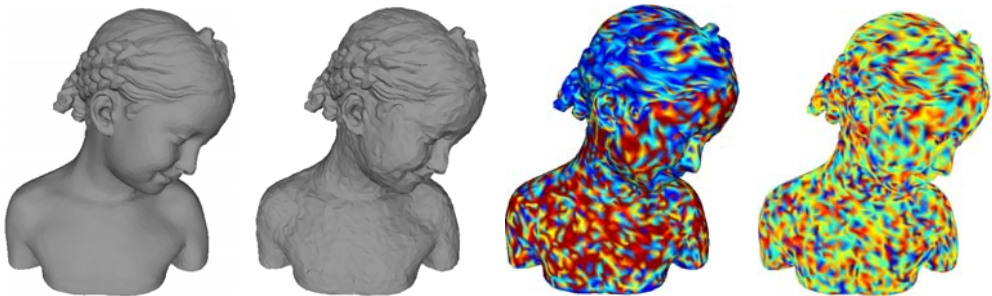


Fig. 7. From left to right: the original Bimba model, the distorted Bimba model after uniform random noise addition, the distance map of *TPDM* between the two meshes, and the distance map of *RMS*. In the distances maps, warmer colors represent higher local distance values.

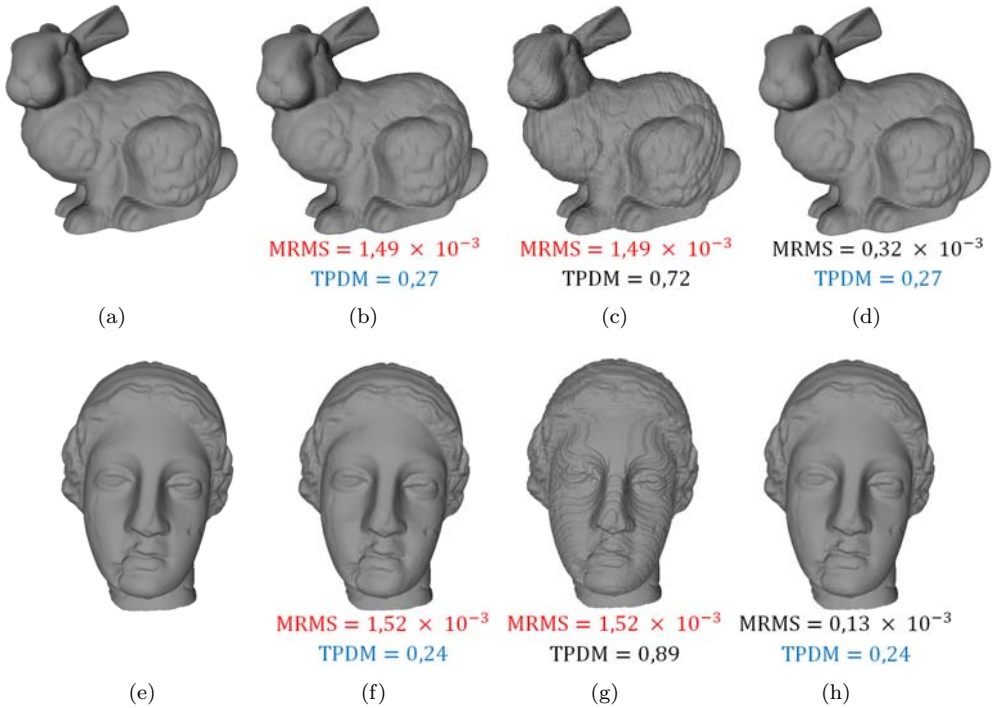


Fig. 8. Application of *TPDM* to the perceptual evaluation of robust mesh watermarking: (a)- original Bunny model; (b)- Bunny watermarked by using the method in [33]; (c)- and (d)- models watermarked by the method in [21] giving, respectively, the same *MRMS* and *TPDM* distortion as (b); (e)- original Venus model; (f)- Venus watermarked by the method in [33]; (g)- and (h)- models watermarked by the method in [21], giving, respectively, the same *MRMS* and *TPDM* distortion as (f). The *TPDM* values are those obtained after psychometric fitting.

4.2. Applications

In this subsection, we show two simple examples to illustrate the potential of *TPDM* in practical mesh applications. The two examples concern, respectively, the quality evaluation of watermarked meshes and the optimum quantization level selection for mesh vertex coordinates.

Figure 8 shows the potential application of our metric *TPDM* in the visual quality assessment of watermarked meshes or, more generally, in the benchmarking of robust mesh watermarking algorithms. Indeed, when comparing two robust watermarking algorithms, a common strategy is to first of all fix the amount of distortion induced by watermark embedding, and then compare the robustness of watermarks against a series

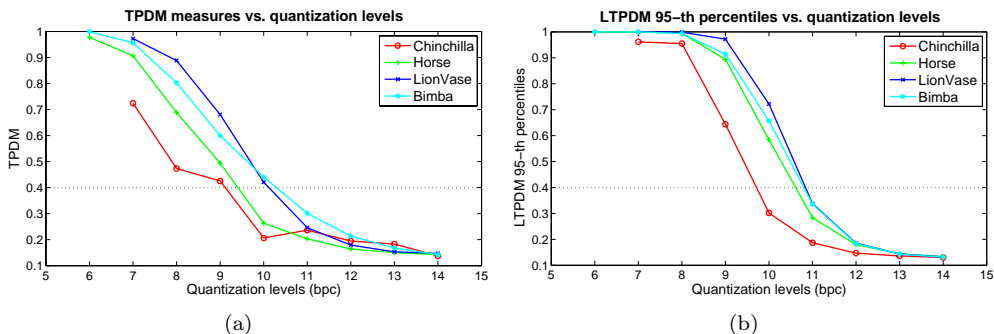


Fig. 9. Application of $TPDM$ for the selection of optimum quantization level of mesh vertex coordinates: (a)- $TPDM$ versus quantization levels, with threshold $\tau_{TPDM} = 0.40$; and (b)- 95-th percentiles of $LTPDM$ versus quantization levels, with threshold $\tau_{LTPDM} = 0.40$.

of attacks, such as noise addition, smoothing and simplification. The question comes to how to quantify the induced distortion. We consider that using classical mesh geometric distances (e.g., maximum root mean squared error, $MRMS$ [6, 11]) is not appropriate, at least when the watermarked meshes are used in applications having human beings as users. In Figs. 8(b) and 8(f) (second column of the figure) we show two watermarked models generated by the method of Wang et al. [33]. We show in Figs. 8(c) and 8(g) (third column) the corresponding watermarked models produced by the method of Cho et al. [21] that have exactly the same $MRMS$ as Wang et al.'s models. Despite having the same $MRMS$ values, the watermarked models produced by the two methods are of significantly different visual quality, and so it would be unfair to conduct robustness comparison on these models. In contrast, the comparison would be fair enough, at least for applications where the visual quality of watermarked mesh is very important, if we fix the amount of $TPDM$ distortion induced by the two methods. We show in Figs. 8(d) and 8(h) (last column) the watermarked models produced by the method of Cho et al. [21] that have exactly the same $TPDM$ values as the models of Wang et al. The watermarked meshes are of comparable and good visual quality.

The second potential application of $TPDM$ shown here is automatic selection of the optimum quantization level of mesh vertex coordinates, defined as the minimum number of bits allocated for representing each quantized coordinate that does not introduce unacceptable visual distortion. Vertex coordinate quantization is almost a mandatory step in lossy mesh compression, but the selection of optimum quantization level is in general mesh-dependent and tedious, which often requires efforts of human observers. $TPDM$ could help us facilitate this task. For this purpose, we introduce two kinds of thresholds, as explained below. The first threshold τ_{TPDM} is defined on the global $TPDM$ value, which guarantees good global visual quality of the mesh after quantization. In Fig. 9(a)

we plot $TPDM$ values versus quantization levels for four meshes of different geometric complexity, and the threshold (i.e., the maximum allowable $TPDM$ introduced by quantization) is fixed as 0.40. The second threshold τ_{LTPDM} is defined on the local tensor-based perceptual distance measures, so as to ensure precise control of the local distortion. For this local control, we first compute the 95-th percentile of the $LTPDM$ distances after quantization (i.e., the value below which 95 percent of $LTPDM$ distances may be found in a quantized mesh), and then compare this percentile value with τ_{LTPDM} . In Fig. 9(b) we show the 95-th percentiles of $LTPDM$ versus quantization levels, and the threshold τ_{LTPDM} is fixed as 0.40, the same value as τ_{TPDM} . Compared to the global threshold, the local threshold appears to be a more strict metric for the control of introduced distortion. We show the quantization results in Fig. 10. For Chinchilla and Bimba, both global and local thresholds select the same level as the optimum, i.e., 10 *bpc* (*bits per coordinate*) for Chinchilla and 11 *bpc* for Bimba, which are consistent with human perception. For Horse, after applying the global threshold, a relatively low quantization level 10 *bpc* is selected, which results in a mesh of rather globally acceptable visual quality, but with some high-amplitude local distortions (especially on the head); the local threshold is stricter and selects 11 *bpc* as the optimum, so as to avoid visually unacceptable local distortion. Another remark is that $TPDM$ may result in unstable assessment results for meshes with relatively few vertices. As shown in Fig. 9(a), for Chinchilla, which has 4307 vertices, the distorted mesh obtained after 10-bit quantization is of better quality than the mesh obtained after 11-bit quantization, according to the $TPDM$ values. Although the two meshes are of rather comparable visual quality (cf. Figs. 10(b) and 10(c)), we think that this is a drawback of the proposed metric, and an improvement on this point will be part of our future work.

5. Conclusion and Future Work

A new curvature-tensor-based approach to objective evaluation of visual mesh quality has been proposed. We show that it is beneficial to use the information on both the curvature amplitudes and the principal curvature directions for MVQ assessment. The local tensor distance that we propose may be found useful in other mesh applications, such as mesh segmentation and shape matching. Experimental results show that our $TPDM$ metric has high correlation with subjective scores and performance comparable with the best performing MVQ metrics proposed so far. Finally, two simple examples illustrate the potential applications of the proposed metric.

$TPDM$ implementation is freely available on-line at <http://www.gipsa-lab.fr/~fakhri.torkhani/software/TPDM.rar>. Future work will consist mainly in integrating more HVS features into the metric (e.g., the contrast sensitivity function), extending the metric to perceptual evaluation of triangular meshes with photometric properties (i.e., with color and textures), and developing a curvature-tensor-based visual quality

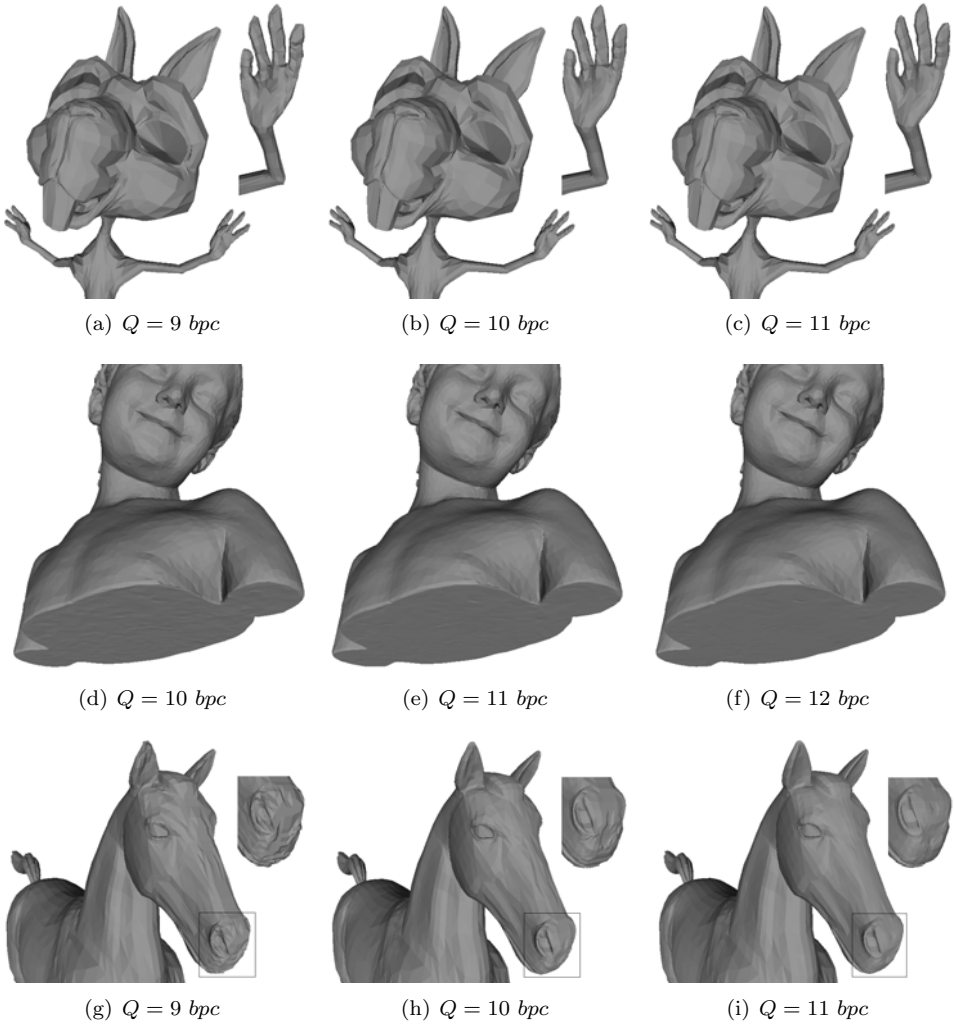


Fig. 10. Application of *TPDM* to the selection of optimum quantization level of mesh vertex coordinates. For Chinchilla (first row, (a)-(c)), both global and local thresholds select 10 *bpc* as the optimum level (Q in bits per coordinate). For Bimba (second row, (d)-(f)), both global and local thresholds select 11 *bpc* as the optimum level. For Horse (third row, (g)-(i)), the global threshold selects 10 *bpc* as the optimum level while the local threshold selects 11 *bpc* as the optimum level.

metric for dynamic meshes. In particular, for perceptual evaluation of dynamic meshes, it would be interesting to derive a spatial-temporal perceptually-oriented curvature tensor distance that accounts for both the spatial visual masking effect (as shown in this paper) and the temporal visual masking effect due to the movement of the 3D mesh.

References

- 1927**
[1] A. Michelson. *Studies in Optics*. Univ. of Chicago Press.
- 1969**
[2] H. S. M. Coxeter. *Introduction to Geometry, 2nd Ed.* Wiley.
- 1985**
[3] M. Brady, J. Ponce, A. L. Yuille, and H. Asada. Describing surfaces. *Comput. Vision, Graphics, and Image Process.*, 32(1):1–28.
- 1993**
[4] H. Kukkonen, J. Rovamo, K. Tiippana, and R. Näsänen. Michelson contrast, RMS contrast and energy of various spatial stimuli at threshold. *Vision Research*, 33(10):1431–1436.
- 1995**
[5] M. C. Morrone, D. C. Burr, and L. M. Vaina. Two stages of visual processing for radial and circular motion. *Nature*, 376(6540):507–509.
- 1998**
[6] P. Cignoni, C. Rocchini, and R. Scopigno. Metro: measuring error on simplified surfaces. *Comput. Graphics Forum*, 17(2):167–174.
- 2000**
[7] P. G. Engeldrum. *Psychometric Scaling: A Toolkit for Imaging Systems Development*. Imcotek Press.
[8] A. Hertzmann and D. Zorin. Illustrating smooth surfaces. In *Proc. of ACM Siggraph*, pages 517–526.
[9] Z. Karni and C. Gotsman. Spectral compression of mesh geometry. In *Proc. of ACM Siggraph*, pages 279–286.
- 2001**
[10] B.-E. Rogowitz and H.-E. Rushmeier. Are image quality metrics adequate to evaluate the quality of geometric objects. In *Proc. of Human Vision and Electronic Imaging*, pages 340–348.
- 2002**
[11] N. Aspert, D. Santa-Cruz, and T. Ebrahimi. MESH: measuring errors between surfaces using the Hausdorff distance. In *Proc. of IEEE Int. Conf. on Multimedia & Expo*, pages 705–708.
- 2003**
[12] P. Alliez, D. Cohen-Steiner, O. Devillers, B. Lévy, and M. Desbrun. Anisotropic polygonal remeshing. *ACM Trans. on Graphics*, 22(3):485–493.
[13] D. Cohen-Steiner and J. M. Morvan. Restricted Delaunay triangulations and normal cycle. In *Symp. on Computational Geometry*, pages 312–321.
[14] O. Sorkine, D. Cohen-Or, and S. Toledo. High-pass quantization for mesh encoding. In *Proc. of Eurographics/ACM Siggraph Symp. on Geometry Processing*, pages 42–51.
[15] Z. Wang and X. Shang. Spatial pooling strategies for perceptual image quality assessment. In *Proc. of IEEE Int. Conf. on Image Process.*, pages 2945–2948.
- 2004**
[16] Z. Wang, A. C. Bovik, H. R. Sheikh, and E. P. Simoncelli. Image quality assessment: From error visibility to structural similarity. *IEEE Trans. on Image Process.*, 13(4):600–612.
- 2006**
[17] G. Lavoué, E. Drelie Gelasca, F. Dupont, A. Baskurt, and T. Ebrahimi. Perceptually driven 3D distance metrics with application to watermarking. In *Proc. of SPIE Electronic Imaging*, pages 63120L.1–63120L.12.

- [18] O. Sorkine. Differential representations for mesh processing. *Comput. Graphics Forum*, 25(4):789–807.
- [19] Z. Wang and A. C. Bovik. *Modern Image Quality Assessment*. Morgan & Claypool.
2007
- [20] B. G. Breitmeyer. Visual masking: past accomplishments, present status, future developments. *Advances in Cognitive Psychology*, 3(1-2):9–20.
- [21] J.-W. Cho, R. Prost, and H.-Y. Jung. An oblivious watermarking for 3-D polygonal meshes using distribution of vertex norms. *IEEE Trans. on Signal Process.*, 55(1):142–155.
- [22] M. Corsini, E. Drelie Gelasca, T. Ebrahimi, and M. Barni. Watermarked 3-D mesh quality assessment. *IEEE Trans. on Multimedia*, 9(2):247–256.
2008
- [23] F. Cole, A. Golovinskiy, A. Limpaecher, H.-S. Barros, A. Finkelstein, T. Funkhouser, and S. Rusinkiewicz. Where do people draw lines? *ACM Trans. on Graphics*, 27(3):88:1–88:11.
- [24] B. Vallet and B. Lévy. Spectral geometry processing with manifold harmonics. *Comput. Graphics Forum*, 27(2):251–260.
2009
- [25] Z. Bian, S.-M. Hu, and R. R. Martin. Evaluation for small visual difference between conforming meshes on strain field. *J. of Comput. Sci. and Technol.*, 24(1):65–75.
- [26] G. Lavoué. A local roughness measure for 3D meshes and its application to visual masking. *ACM Trans. on Appl. Perception*, 5(4):21:1–21:23.
- [27] Q. Li and Z. Wang. Reduced-reference image quality assessment using divisive normalization-based image representation. *IEEE J. Sel. Topics Signal Process.*, 3(2):202–211.
- [28] S. Silva, B. S. Santos, C. Ferreira, and J. Madeira. A perceptual data repository for polygonal meshes. In *Proc. of Int. Conf. in Visualization*, pages 207–212.
- [29] Z. Wang and A. C. Bovik. Mean squared error: love it or leave it? — A new look at signal fidelity measures. *IEEE Signal Process. Magazine*, 26(1):98–117.
2010
- [30] M. Botsch, L. Kobbelt, M. Pauly, P. Alliez, and B. Lévy. *Polygon Mesh Processing*. AK Peters, 2010.
- [31] G. Lavoué and M. Corsini. A comparison of perceptually-based metrics for objective evaluation of geometry processing. *IEEE Trans. on Multimedia*, 12(7):636–649.
2011
- [32] G. Lavoué. A multiscale metric for 3D mesh visual quality assessment. *Comput. Graphics Forum*, 30(5):1427–1437.
- [33] K. Wang, G. Lavoué, F. Denis, and A. Baskurt. Robust and blind mesh watermarking based on volume moments. *Comput. & Graphics*, 35(1):1–19.
- [34] Z. Wang and A. C. Bovik. Reduced- and no-reference image quality assessment. *IEEE Signal Process. Magazine*, 28(6):29–40.
2012
- [35] P. Alliez, S. Tayeb, and C. Wormser. 3D fast intersection and distance computation (AABB tree). In *CGAL User and Reference Manual*.
- [36] F. Torkhani, K. Wang, and J.-M. Chassery. A curvature tensor distance for mesh visual quality assessment. In *Proc. of Int. Conf. on Computer Vision and Graphics*, pages 253–263.
- [37] L. Váša and J. Rus. Dihedral angle mesh error: a fast perception correlated distortion measure for fixed connectivity triangle meshes. *Comput. Graphics Forum*, 31(5):1715–1724.
- [38] K. Wang, F. Torkhani, and A. Montanvert. A fast roughness-based approach to the assessment of 3D mesh visual quality. *Comput. & Graphics*, 36(7):808–818, 2012.
2013
- [39] M. Corsini, M.C. Larabi, G. Lavoué, O. Petřík, L. Váša, and K. Wang. Perceptual metrics for static and dynamic triangle meshes. *Comput. Graphics Forum*, 32(1):101–125. (Improved version of Eurographics 2012 state-of-the-art report).
- [40] G. Lavoué. Erratum of the Results of Mesh Visual Quality Metrics (Available on-line at <http://liris.cnrs.fr/glavoue/travaux/Erratum.html>), 2013.